Structure and dynamics of C_{60} molecules in liquid CS_2 from neutron scattering

H. E. Smorenburg, R. M. Crevecoeur, I. M. de Schepper, and L. A. de Graaf
Interfacultair Reactor Instituut, Delft University of Technology, 2629 JB Delft, The Netherlands
(Received 28 March 1995)

By means of inelastic neutron scattering we determine the dynamic structure factors $S(k,\omega)$ of two dilute suspensions of C_{60} molecules dissolved in liquid CS_2 (C_{60} number densities 0.0034 and 0.0067 nm^{-3}) at 1 bar and 293 K for wave numbers $1<k<15$ nm^{-1} and high energy resolution $\Delta\omega \geq 0.0015$ ps^{-1}. $S(k,\omega)$ can be described by a sum of a narrow and a broad Lorentzian. The intensity of the narrow Lorentzian agrees perfectly with that calculated for a single C_{60} molecule. The area of the broader line is in good agreement with that obtained from fluctuations in the total number density of the mixture. This contribution is small for $k<5$ nm^{-1}, but it dominates for $k>7$ nm^{-1}. From the widths of the narrow Lorentzians we find the diffusion coefficient of C_{60} in CS_2, $D_S=1.04\times10^{-9}$ $m^2 s^{-1}$, significantly smaller than those obtained from the Stokes-Einstein relation (1.30×10^{-9} m^2 s^{-1}) and the kinetic theory for binary mixtures (1.5×10^{-9} m^2 s^{-1}).

PACS number(s): 61.12.−q, 66.10.Cb, 05.20.Dd

I. INTRODUCTION

The dynamics of dilute monodisperse suspensions of neutral spherical colloidal particles in a solvent has been extensively studied by means of dynamic light scattering techniques [1]. The quantity that is in fact obtained is the coherent dynamic structure factor $S(k,\omega)$ of the colloidal particles as a function of wave number k and frequency ω.

At very low volume fractions $\phi<0.01$ (with $\phi=\pi n\sigma^3/6$, n the number density of the colloidal particles, and σ their diameter, typically $10<\sigma<1000$ nm), $S(k,\omega)$ is for practically all k described by one Lorentzian line in ω with a k-dependent half-width $\omega_H(k)=D_{SE}k^2$. Here D_{SE} is the Stokes-Einstein diffusion coefficient of one colloidal particle at infinite dilution,

$$D_{SE}=\frac{k_BT}{3\pi\eta\sigma}\ , \tag{1}$$

with T the temperature, k_B Boltzmann's constant, and η the shear viscosity of the solvent. The continuum Stokes-Einstein description of $S(k,\omega)$ [cf. Eq. (1)] is expected to break down when the diameter σ of the colloidal particles becomes of the order of that of the fluid particles (typically $\sim$0.3 nm). In that case one must rely theoretically on kinetic theories for binary mixtures and experimentally on inelastic neutron scattering. In particular it has been shown that the spectra obtained from neutron scattering on Ne-He and Ar-He mixtures can be understood very well on the basis of the so-called revised Enskog theory (RET) [2] for binary mixtures of hard spheres [3]. Here the Ne or Ar atoms in the mixture can be considered as heavy spherical "colloidal" particles, with a diameter σ however, which is not more than about 30% larger than the diameter of the He, "solvent" atoms. Although the RET can describe such colloidlike mixtures, it *cannot* be extended to real colloidal suspensions ($\sigma>10$ nm) since it does *not* lead to Eq. (1) for the diffusion coefficient of one heavy particle in the solvent [4].

In this paper we study the dynamic behavior of a system that is intermediate between a colloidal suspension and a binary mixture such as Ar-He. We do so to investigate the usefulness of the Stokes-Einstein and kinetic theory descriptions in the intermediate region $0.5<\sigma<10$ nm, where *both* might be relevant but where both theories are not obviously valid. Therefore we consider at room temperature $T=293$ K two solutions of C_{60} molecules ("fullerenes") dissolved in liquid CS_2 with number density $n_{CS_2}=10$ nm^{-3} and C_{60} number densities $n_{C_{60}}=0.0034$ and 0.0067 nm^3. Each of these systems is a dilute essentially monodisperse solution of perfect C_{60} spheres with a diameter $\sigma=0.91$ nm [5], which is considerably larger than the effective diameter of the solute particles (0.42 nm) [5] and in the region $0.5<\sigma<10$ nm of present interest. We use CS_2, since its effective diameter is the smallest among the solvents in which C_{60} molecules can be dissolved sufficiently [6] to be actually measured by neutron scattering. We consider two solutions of C_{60} particles to study the dependence on the number density $n_{C_{60}}$, in particular to see whether the C_{60} molecules move independently of each other.

We show that quasielastic neutron scattering is suited for studying the dynamics of these C_{60}-CS_2 systems. At small wave numbers $k\approx1$ nm^{-1}, $S(k,\omega)$ is dominated by the contribution of the slowly moving C_{60} molecules. Then $S(k,\omega)$ should be measured with an energy resolution of about $\Delta\omega\leq2\omega_H(k)\sim2D_{SE}k^2\sim0.003$ ps^{-1} [cf. Eq. (1) with $\eta=0.363\times10^{-3}$ $kg\,m^{-1}s^{-1}$ for CS_2 [7]]. Such high energy resolutions can be achieved with the inelastic neutron scattering IRIS spectrometer of ISIS (Rutherford Appleton Laboratory, United Kingdom). For increasing k the C_{60} contribution widens and in addition one starts to observe the faster motion of the CS_2 molecules. Then larger energy resolutions may be used.

Using the IRIS spectrometer, it appears for all k that

$S(k,\omega)$ can be described by a narrow Lorentzian in ω (mainly due to the heavy C_{60} molecules dominating for $k<5$ nm^{-1}) and a broad Lorentzian (mainly due to the CS_2 molecules dominating for $k>7$ nm^{-1}). Their intensities as a function of k are in good agreement with those calculated for a binary mixture of hard spheres with noncentral scattering centers as in the actual molecules. The half-widths of the two Lorentzians in $S(k,\omega)$ agree only qualitatively with those calculated from the revised Enskog theory. For both solutions we obtain a diffusion coefficient of the C_{60} molecules in CS_2, $D_S=1.04\times10^{-9}$ m^{2}s^{-1}, which is significantly smaller than that obtained from the Stokes-Einstein equation [Eq. (1)] $D_{SE}=1.3\times10^{-9}$ m^{2}s^{-1} and from the revised Enskog theory $D_E=1.5\times10^{-9}$ m^{2}s^{-1}.

This paper is organized as follows. In Sec. II we describe the neutron scattering experiment, show typical inelastic neutron scattering spectra $I(k,\omega)$ from which $S(k,\omega)$ is determined, and present the results for the k-dependent intensities and half-widths that describe $S(k,\omega)$. In Sec. III we summarize the theory for the structure and dynamics of binary mixtures of hard sphere molecules and compare with experiment. We end with a discussion in Sec. IV.

II. EXPERIMENT

We discuss the sample preparation (Sec. II A), the neutron spectrometer (Sec. II B), the data collection (Sec. II C), and give the experimental results (Sec. II D).

A. Sample

We prepared two solutions of C_{60} in CS_2 following the recipe described by Ruoff *et al.* [6]. Pure C_{60} (Syncom, greater than 99.9%) was weighed and dissolved in CS_2 (BDH, greater than 99.9%). After stirring 12 h in the dark, 20 ml of the solutions (with 4.0 and 7.9 mg C_{60}/ml CS_2, respectively) were transferred to aluminum cylindrical sample cans (inner diameter 20 mm) used in the neutron scattering experiments. The corresponding number densities of the C_{60} molecules are $n_{C_{60}}=0.0034$ and 0.0067 nm^{-3}, respectively. Since CS_2 is extremely volatile and reactive with rubber, the sample cans were sealed with Teflon O rings and tested by weighing to be leak proof. During the preparation and experiments the samples were kept at room temperature.

B. Spectrometer

The experiments were performed on the spectrometer IRIS at the pulsed neutron source ISIS. IRIS is a so-called time of flight inverted-geometry spectrometer, which can achieve energy resolutions up to 0.0015 ps^{-1} (full width at half maximum) by using the (002) reflection of mica analyzers in nearly backscattering geometry [8]. The analyzed neutron wavelength is $\lambda_{MC002}=2.0$ nm, so that the smallest momentum transfer $k_{min}=4\pi\sin(\phi_{min}/2)/\lambda_{MC002}=1.3$ nm^{-1} with $\phi_{min}=24.00°$ the smallest angle at which spectra can be measured. Employing the full intensity of ISIS, using the 50-Hz mode, the energy transfer is limited to $-0.025<\omega<0.025$ ps^{-1} due to frame overlap of two subsequent pulses. We have extended the energy transfer range considerably by using the mica (MC) (004) and pyrolytic graphite (PG) (002) analyzer reflections, with analyzed wavelengths $\lambda_{MC004}=1.0$ nm and $\lambda_{PG002}=0.667$ nm, respectively. In these modes we have an energy transfer range of $-0.25<\omega<0.25$ ps^{-1} for mica (004) and $-0.75<\omega<0.75$ ps^{-1} for PG (002), whereas the energy resolutions are $\Delta\omega\approx0.0075$ and 0.025 ps^{-1}, respectively. In this way a large momentum and energy transfer range with sufficiently high energy and momentum transfer resolution is covered. The properties of the IRIS spectrometer are summarized in Table I.

TABLE I. Settings of the IRIS spectrometer in 50-Hz mode with symmetric energy windows, for analyzer crystals, analyzed wavelength λ, energy resolution $\Delta\omega$, maximum energy transfer ω_{max} ("energy window"), and minimum wave number k_{min}.

Analyzer	λ (nm)	$\Delta\omega$ (ps^{-1})	ω_{max} (ps^{-1})	k_{min} (nm^{-1})
MC002	2.0	0.0018	0.025	1.3
MC004	1.0	0.0073	0.25	2.6
PG002	0.67	0.025	0.75	4.4

C. Data collection

For the 7.9-mg/ml sample we determined the neutron intensities $I_j(\phi,t)$ as a function of scattering angle ϕ and time of flight t for the C_{60}-CS_2 system using the mica (002) reflection for 53 h (j=MC002), the mica (004) reflection for 33 h (j=MC004), and the pyrolytic graphite (002) (j=PG002) reflection for 13 h. For the 4.0-mg/ml sample we used the mica (004) reflection 9 h. We also determined the corresponding spectra $I_j^{CS_2}(\phi,t)$ of pure CS_2 for both mica reflections in 17 and 10 h, respectively. Due to a failure of the ISIS spallation source we could not measure the pure CS_2 spectra in the PG (002) mode. By following the neutron intensities in the course of time (in steps of a few hours) we found that the sample and the performance of the spectrometer did not change during the full experiment and that the spectra were reproducible.

In our experiment a constant scattering angle ϕ corresponds to a constant wave number $k=4\pi\lambda_j^{-1}\sin(\phi/2)$ for all j, since the energy transfer is very small. The time of flight t is used to calculate the energy transfer ω from the neutron to the sample (positive ω corresponds to energy gain in the sample). Thus we write $I_j(\phi,t)$ and $I_j^{CS_2}(\phi,t)$ henceforth as $I_j(k,\omega)$ and $I_j^{CS_2}(k,\omega)$. In Fig. 1 we show spectra $I_j(k,\omega)$ for $k=1.3$ nm^{-1} (j=MC002) and $k=3.8$ nm^{-1} (j=MC004). The dashed lines in Figs. 1(a) and 1(b) are the corresponding CS_2 data $I_j^{CS_2}(k,\omega)$. Around $\omega=0$ one observes a tiny narrow contribution due to the incoherent elastic scattering from the Al sample can. In Fig. 2 the sample $I_j(k,\omega)$ (j=PG002) are shown for $k=5.6$, 7.3, 10.1, and 12.4 nm^{-1}. Note the strong broadening of the spectra for increasing k in Figs.

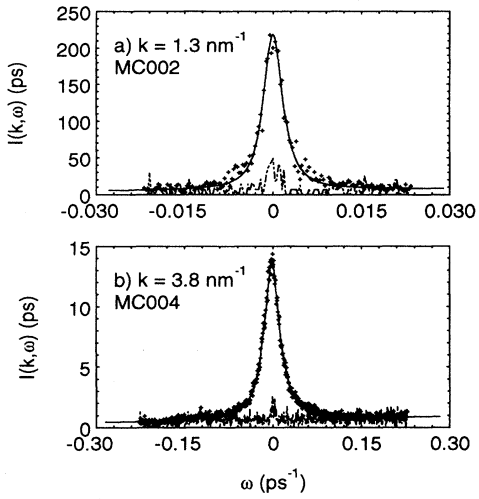

FIG. 1. Neutron intensities $I(k,\omega)$ as functions of ω for $k=1.3$ (a) and 3.8 nm^{-1} (b): C_{60} in CS_2 (7.9 mg/ml), crosses; pure CS_2, dashed curve; best Lorentzian fit [cf. Eqs. (2) and (3)], solid curve.

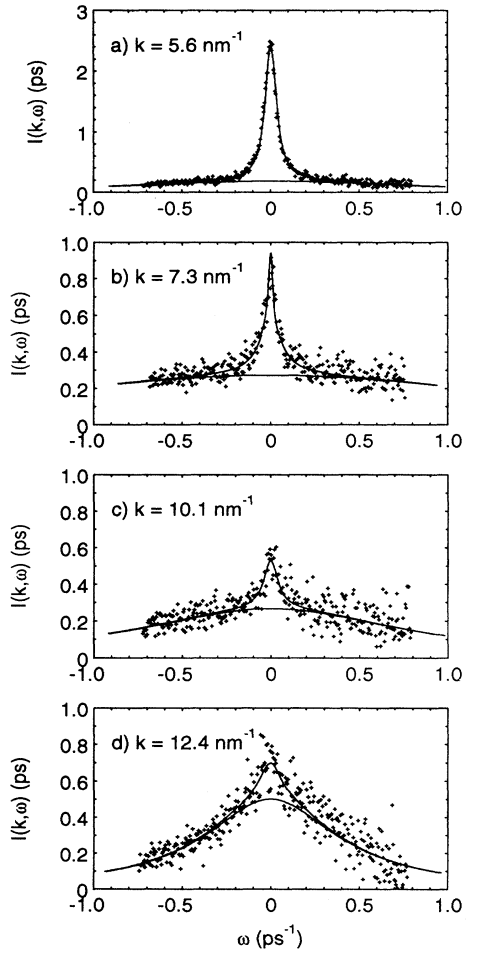

FIG. 2. Neutron intensities $I(k,\omega)$ as a functions of ω for $k=5.6$ (a), 7.3 (b), 10.1 (c), and 12.4 nm^{-1} (d) of C_{60} in CS_2 (7.9 mg/ml) (crosses). The upper curve shows the best two Lorentzian fits [cf. Eqs. (2) and (3)]. The lower solid curve is the Lorentzian contribution from fluctuations in the total number (N) density (i.e., from the solvent).

1(a), 1(b), and 2.

In order to determine the resolution functions $R_j(k,\omega)$ (j=MC002, MC004, and PG002) of the spectrometer and the efficiencies of the detectors $E_j(k)$, we performed measurements on an elastically, incoherently scattering sample with the same geometry as the C_{60}-CS_2 sample. For mica (004) and PG (002) vanadium was used, but for mica (002) we used a polythene sample since the absorption cross section of vanadium for these long wavelengths (analyzed wavelength $\lambda_{MC002}=2.0$ nm) is rather high. After correction for self-shielding [9] we find the relative efficiency of each detector $E_j(k)$ and the normalized resolution functions $R_j(k,\omega)$ [$\int d\omega R_j(k,\omega)=1$]. At fixed j, the efficiencies $E_j(k)$ are used to normalize the spectra $I_j(k,\omega)$ relative to one another for varying k values. The spectra $I_j(k,\omega)$ are normalized relatively to each other for varying j=MC002, MC004, and PG002 by equating the spectra at overlapping k values. Thus the intensities of the spectra shown in Figs. 1 and 2 can be compared with one another.

The energy resolutions $\Delta\omega_j(k)$ [i.e., the full width at half maximum of $R_j(k,\omega)$] are $0.0017<\Delta\omega_{MC002}(k)<0.0020$ ps^{-1} for mica (002), $0.0067<\Delta\omega_{MC004}(k)<0.0079$ ps^{-1} for mica (004), and $\Delta\omega_{PG002}(k)=0.025$ ps^{-1} for PG (002). They increase slightly (and approximately linearly) from the smallest to the largest scattering angle, due to the finite size of the sample can. The correction for the resolution is taken into account in the fitting procedure.

D. Results

The neutron spectra are given by

$$I_j(k,\omega)=\int_{-\infty}^{+\infty} d\omega'[S_{expt}(k,\omega')+c_j\delta(\omega')+b_j(k,\omega')] \times R_j(k,\omega-\omega') , \quad (2)$$

with j=MC002, MC004, and PG002. $c_j\delta(\omega)$ represents the (weak) incoherent elastic scattering from the aluminum sample can [see Figs. 1(a) and 1(b), dashed lines], which is assumed to be constant for each j. The function $b_j(k,\omega)$ is for each j and k a linear function of ω, effectively representing the very small background scattering that is observed at $\omega\gg 0$ and $\omega\ll 0$. $S_{expt}(k,\omega)$ is the experimental dynamic structure factor of the C_{60}-CS_2 system.

We find that the ω dependence of $I_j(k,\omega)$ can be described by $S_{expt}(k,\omega)$, which consists of a narrow and a broad Lorentzian line in ω, with labels c and N, respectively, i.e.,

$$S_{expt}(k,\omega)=I_c(k)\frac{\omega_c(k)/\pi}{\omega_c(k)^2+\omega^2}+I_N(k)\frac{\omega_N(k)/\pi}{\omega_N(k)^2+\omega^2} \quad (3)$$

with k-dependent areas $I_c(k)$ and $I_N(k)$ and half-widths $\omega_c(k)$ and $\omega_N(k)$. We will show in Sec. III that these two Lorentzians are due to fluctuations in the concentration (label c) and total density (label N). Absolute normalization of the spectra is obtained from the property that for $k\to\infty$, $\int d\omega S_{expt}(k,\omega)=1$, as will be discussed in Sec. III.

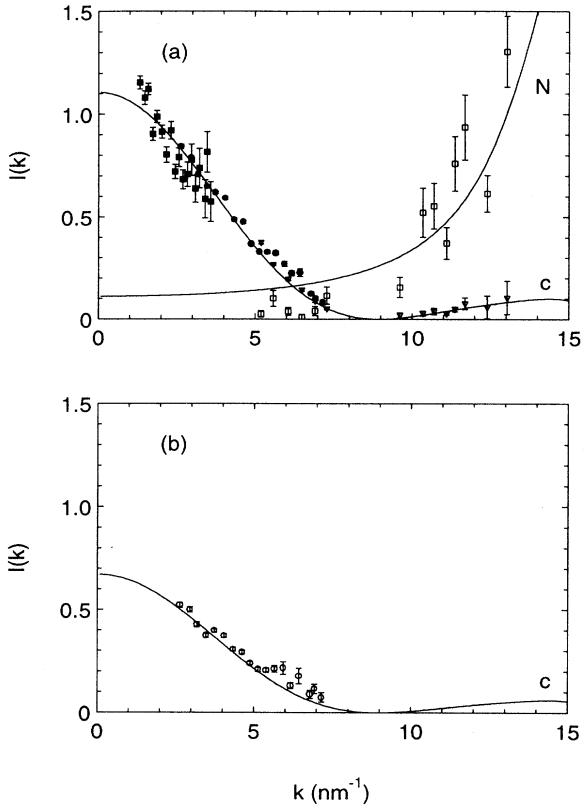

FIG. 3. Neutron intensities $I_N(k)$ and $I_c(k)$ as functions of k for C_{60} in CS_2 at (a) 7.9 mg/ml and (b) 4.0 mg/ml. (a) Experiment: for $I_c(k)$, MC002, (■), MC004 (●), PG002 (▽); for $I_N(k)$, PG002 (□). (b) Experiment: for $I_c(k)$, MC004 (○). The solid curves are theoretical for hard spheres [cf. Eq. (42)].

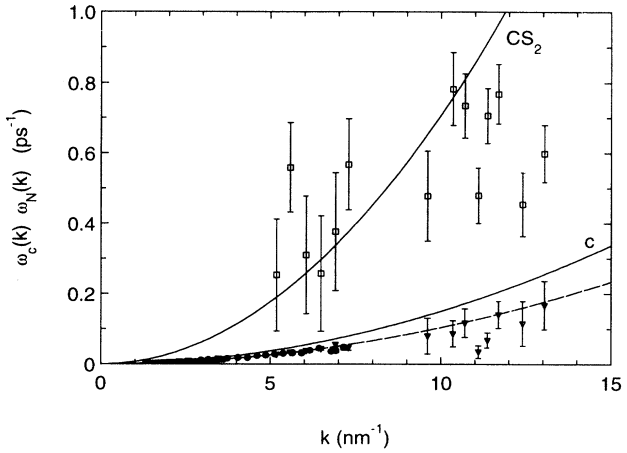

FIG. 4. Neutron half-widths $\omega_c(k)$ and $\omega_N(k)$ as functions of k for C_{60} in CS_2 at 7.9 mg/ml. Experiment: for $\omega_N(k)$, PG002 (□); for $\omega_c(k)$, PG002 (▽), MC004 (●), and MC002 (■). The solid curves $\omega_{CS_2}(k)$ and $\omega_c(k)$ are from the Enskog theory (cf. Fig. 8). The dashed line is the best fit $\omega_c(k)=D_S k^2$ with $D_S=(1.04\pm0.01)\times10^{-9}$ m^2 s^{-1}.

The energy window covered by the mica reflections [j=MC002 and MC004 (cf. Table I)] is too restricted to observe clearly the broad Lorentzian term (with label N). Then the second term in Eq. (3) is indistinguishable from the linear background term $b_j(k,\omega)$ in Eq. (2) [see Figs. 1(a) and 1(b)]. Only the PG (002) energy window (cf. Table I) is large enough to observe clearly a second Lorentzian (see Fig. 2).

For the 7.9-mg/ml solution the fitted areas $I_c(k)$ and $I_N(k)$ are shown in Fig. 3(a). $I_c(k)$ is plotted with solid squares (j=MC002), dots (j=MC004), and triangles (j=PG002), whereas the $I_N(k)$ is plotted with open squares. The intensities $I_c(k)$ scattered by the 4.0-mg/ml solution are plotted in Fig. 3(b). The 4.0-mg/ml solution scatters clearly less (about 50%) than the 7.9-mg/ml solution. In Fig. 4 the half-widths $\omega_c(k)$ and $\omega_N(k)\gg\omega_c(k)$ are plotted as a function of k for the 7.9-mg/ml solution. The widths $\omega_N(k)$ (open squares) are in the order of 0.5 ps^{-1}, which is about the energy range that could be reached with the PG002 analyzers (see Fig. 2). This causes a large spread (and possibly systematic errors) in the fitted intensities $I_N(k)$ [see Fig. 3(a)] and half-widths $\omega_N(k)$ (see Fig. 4). Three dead detectors between $49°<\phi<52°$ are the reason for missing data between $7.5<k<9.5$ nm^{-1} in Figs. 3 and 4. In Fig. 5 we show the half-widths $\omega_c(k)$ as a function of k for the 4.0-mg/ml (circles) and 7.9-mg/ml solutions (squares, dots, and triangles) on a double logarithmic scale. The half-widths of the 4.0-mg/ml solution do not significantly differ from those obtained from the 7.9-mg/ml solution, although the statistical errors are larger due to the intrinsically lower intensity and the shorter measuring time. The half-widths in Fig. 5 are represented very well by $\omega_c(k)=D_S k^2$ with $D_S=(1.04\pm0.01)\times10^{-9}$ m^2 s^{-1} the self-diffusion coefficient of one C_{60} molecule (straight dashed line in Fig. 5).

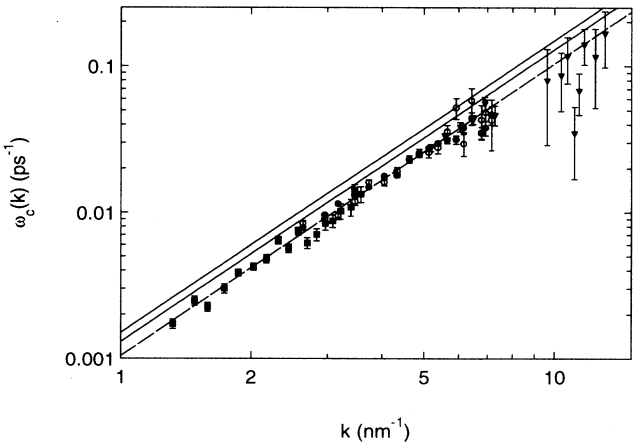

FIG. 5. Neutron half-widths $\omega_c(k)$ as functions of k for C_{60} in CS_2. Experiment: for 7.9 mg/ml, PG002 (▽); MC004 (●), and MC002 (■); for 4.0 mg/ml, MC004 (○). The straight lines are $\omega_c(k)=Dk^2$ with, from top to bottom, $D=D_c^E$ (Enskog), $D=D_{SE}$ (Stokes-Einstein), and $D=D_S$ (best fit).

III. THEORY

We discuss the theory of binary molecular mixtures in Sec. III A, the continuum approximation for the neutron intensities in Sec. III B, specify the theory to the present C_{60}-CS_2 mixtures in Sec. III C, and compare the theoretical results with experiment in Sec. III D.

A. Binary molecular mixtures in general

We extend straightforwardly the general theory described by Lovesey [10] for the static structure factor of a one-component molecular fluid to the dynamic structure factor of a two-component molecular fluid. We consider, in a volume V, a binary mixture of N_1 (large) molecules of species 1 and N_2 (small) molecules of species 2 with $N=N_1+N_2$ and $x_j=N_j/N$ the mole fraction of species $j=1,2$. Each molecule of species $j=1,2$ consists of Z_j atoms that all scatter coherently with coherent neutron scattering lengths $b_{j,q}$ $(q=1,\ldots,Z_j)$. As a result, the molecules scatter in general both coherently and incoherently.

$S_{\text{expt}}(k,\omega)$ observed in neutron scattering is the Fourier transform of the intermediate dynamic structure factor $I(k,t)$, i.e.,

$$S_{\text{expt}}(k,\omega)=\frac{1}{2\pi}\int_{-\infty}^{+\infty}dt\,\exp(i\omega t)I(k,t) \tag{4}$$

with

$$I(k,t)=\frac{1}{Nb^2}\sum_{j,p,q}\sum_{j',p',q'}b_{j,q}b_{j',q'}\langle\exp\{i\mathbf{k}\cdot[\mathbf{R}_{j,p}(0)-\mathbf{R}_{j',p'}(t)+\mathbf{r}_{j,p,q}(0)-\mathbf{r}_{j',p',q'}(t)]\}\rangle\ . \tag{5}$$

Here b is the average scattering length of the molecules defined by

$$b^2=\sum_{j=1,2}x_j\sum_{q=1}^{Z_j}b_{j,q}^2\ , \tag{6}$$

the angular brackets denote the canonical ensemble average over all atoms, $\mathbf{k}$ is a wave vector with length k, and $\mathbf{r}_{j,p,q}(t)$ is the location at time t of atom $q=1,\ldots,Z_j$ on molecule $p=1,\ldots,N_j$ of species $j=1,2$ relative to the center of mass position $\mathbf{R}_{j,p}(t)$ of the molecule to which it belongs. The intermediate dynamic structure factor is normalized such that $\lim_{k\to\infty}\mathbf{I}(k,t=0)=1$ [cf. Eqs. (5) and (6)]. We write $I(k,t)$ as

$$I(k,t)=I^{\text{coh}}(k,t)+I^{\text{inc}}(k,t)\ , \tag{7}$$

where $I^{\text{coh}}(k,t)$ and $I^{\text{inc}}(k,t)$ are due to coherent and incoherent scattering of the molecules, respectively.

First, we consider $I^{\text{coh}}(k,t)$, which is given by the time correlation function of the microscopic scattering length density

$$I^{\text{coh}}(k,t)=\frac{1}{b^2}\langle\delta\rho(\mathbf{k},0)[\delta\rho(\mathbf{k},t)]^*\rangle\ . \tag{8}$$

Here the angular brackets denote the equilibrium canonical ensemble average over the molecular center of mass positions, the asterisk denotes complex conjugation, and the microscopic scattering length density $\delta\rho(\mathbf{k},t)$ at time t is

$$\delta\rho(\mathbf{k},t)=\sum_{j=1,2}x_j^{1/2}f_j^{\text{coh}}(k)\delta n_j(\mathbf{k},t)\ . \tag{9}$$

The extent of one molecule of species j is represented by the coherent angular averaged molecular form factor

$$f_j^{\text{coh}}(k)=\langle\mathcal{F}_{j,p}(\mathbf{k},t)\rangle_{\text{ang}}\ , \tag{10}$$

with $\mathcal{F}_{j,p}(\mathbf{k},t)$ the microscopic molecular form factor of molecule p of species j at time t,

$$\mathcal{F}_{j,p}(\mathbf{k},t)=\sum_{q=1}^{Z_j}b_{j,q}\exp[i\mathbf{k}\cdot\mathbf{r}_{j,p,q}(t)]\ . \tag{11}$$

The normalized average $\langle\ \rangle_{\text{ang}}$ in Eq. (10) extends over all angular orientations of molecule p so that $f_j^{\text{coh}}(k)$ only depends on $j=1,2$ and k but not on p and t. The microscopic density at time t of molecules of species j in Eq. (9) is given by

$$\delta n_j(\mathbf{k},t)=\frac{1}{\sqrt{N_j}}\sum_{p=1}^{N_j}\exp[i\mathbf{k}\cdot\mathbf{R}_{j,p}(t)]\ . \tag{12}$$

To derive Eq. (8) from Eq. (5) one assumes that the correlation between the orientations of different molecules can be neglected.

In a dense fluid mixture, the time relaxations of the two microscopic densities $\delta n_j(\mathbf{k},t)$ are correlated. They are both determined by the independent decay times of the microscopic concentration $\delta c(\mathbf{k},t)$ and microscopic total number density $\delta N(\mathbf{k},t)$ [11], defined by

$$\begin{aligned}\delta N(\mathbf{k},t)\equiv&[x_2^{1/2}S_{22}(k)-x_2^{1/2}S_{12}(k)]\delta n_1(\mathbf{k},t)\\ \delta N(\mathbf{k},t)\equiv&[x_1^{1/2}S_{22}(k)-x_2^{1/2}S_{12}(k)]\delta n_1(\mathbf{k},t)\\ &+[x_2^{1/2}S_{11}(k)-x_1^{1/2}S_{12}(k)]\delta n_2(\mathbf{k},t)\ ,\end{aligned} \tag{13}$$

where the partial molecular static structure factors $S_{ij}(k)$ are given by

$$S_{ij}(k)\equiv\langle\delta n_i(\mathbf{k},0)[\delta n_j(\mathbf{k},0)]^*\rangle\ . \tag{14}$$

By taking the inverse relations of Eq. (13), one obtains $(j=1,2)$

$$\delta n_j(\mathbf{k},t)=T_j^c(k)\delta c(\mathbf{k},t)+T_j^N(k)\delta N(\mathbf{k},t)\ , \tag{15}$$

with $T_j^N(k)=x_j^{1/2}/S_{cc}(k)$, $T_1^c(k)=[x_2^{1/2}S_{11}(k)-x_1^{1/2}/S_{12}(k)]/S_{cc}(k)$, and $T_2^c(k)=[-x_1^{1/2}S_{22}(k)+x_2^{1/2}/S_{12}(k)]/S_{cc}(k)$, where $S_{cc}(k)=\langle\delta c(\mathbf{k},0)[\delta c(\mathbf{k},0)]^*\rangle$ is the static structure factor for concentration fluctuations.

Thus the microscopic scattering length density $\delta\rho(\mathbf{k},t)$ of Eq. (9) can be written as

$$\delta\rho(\mathbf{k},t)\equiv bC_c(k)\delta c(\mathbf{k},t)+bC_N(k)\delta N(\mathbf{k},t) , \tag{16}$$

with

$$C_c(k)=\frac{1}{b}\sum_{j=1,2} x_j^{1/2} f_j^{\mathrm{coh}}(k) T_j^c(k) ,$$
$$C_N(k)=\frac{1}{b}\sum_{j=1,2} x_j^{1/2} f_j^{\mathrm{coh}}(k) T_j^N(k) \tag{17}$$

the relative dimensionless strengths of concentration and total number fluctuations in $\delta\rho(\mathbf{k},t)$. The coherent intermediate dynamic structure factor $I^{\mathrm{coh}}(k,t)$ in Eq. (8) is then given by

$$I^{\mathrm{coh}}(k,t)=C_c(k)^2F_{cc}(k,t)+C_N(k)^2F_{NN}(k,t)$$
$$+2C_c(k)C_N(k)F_{cN}(k,t) , \tag{18}$$

where

$$F_{cc}(k,t)=\langle \delta c(\mathbf{k},0)[\delta c(\mathbf{k},t)]^*\rangle ,$$
$$F_{NN}(k,t)=\langle \delta N(\mathbf{k},0)[\delta N(\mathbf{k},t)]^*\rangle ,$$

and

$$F_{cN}(k,t)=\langle \delta c(\mathbf{k},0)[\delta N(\mathbf{k},t)]^*\rangle$$

are the time correlation functions of molecular concentration and total number fluctuations.

Next we consider the incoherent contribution $I^{\mathrm{inc}}(k,t)$ to $I(k,t)$ in Eq. (7). $I^{\mathrm{inc}}(k,t)$ is given by

$$I^{\mathrm{inc}}(k,t)=\sum_{j=1,2} x_j F_j^{\mathrm{rot}}(k,t)F_j^{\mathrm{trans}}(k,t) , \tag{19}$$

where

$$F_j^{\mathrm{rot}}(k,t)=\frac{1}{b^2}\{\langle \mathcal{F}_{j,p}(\mathbf{k},0)[\mathcal{F}_{j,p}(\mathbf{k},t)]^*\rangle_{\mathrm{ang}}$$
$$-\langle \mathcal{F}_{j,p}(\mathbf{k},t)\rangle_{\mathrm{ang}}^2\} \tag{20}$$

is due to the rotational motion of one molecule (labeled p) of species $j=1,2$ and

$$F_j^{\mathrm{trans}}(k,t)=\langle \exp\{i\mathbf{k}\cdot[\mathbf{R}_{j,p}(0)-\mathbf{R}_{j,p}(t)]\}\rangle \tag{21}$$

is due to its translational motion. Using Eqs. (20) and (21) in Eq. (7), one obtains the final result for the total intermediate dynamic structure factor

$$I(k,t)=[C_c(k)]^2F_{cc}(k,t)+[C_N(k)]^2F_{NN}(k,t)$$
$$+2C_c(k)C_N(k)F_{cN}(k,t)$$
$$+\sum_{j=1,2} x_j F_j^{\mathrm{rot}}(k,t)F_j^{\mathrm{trans}}(k,t) . \tag{22}$$

The integrated intensity $S_{\mathrm{expt}}(k)$ is given by

$$S_{\mathrm{expt}}(k)\equiv\int_{-\infty}^{+\infty} d\omega\, S_{\mathrm{expt}}(k,\omega)=I(k,t=0) \tag{23}$$

so that

$$S_{\mathrm{expt}}(k)=[C_c(k)]^2S_{cc}(k)+[C_N(k)]^2S_{NN}(k)$$
$$+\sum_{j=1}^{2} x_j F_j^{\mathrm{rot}}(k) , \tag{24}$$

with $F_j^{\mathrm{rot}}(k)\equiv F_j^{\mathrm{rot}}(k,t=0)$, and $S_{NN}(k)=F_{NN}(k,0)=\langle \delta N(\mathbf{k},0)[\delta N(\mathbf{k},0)]^*\rangle$ is given by Eqs. (13) and (14).

To derive Eq. (24) we have used that for all k, $F_{cN}(k,0)=\langle \delta c(\mathbf{k},0)[\delta N(\mathbf{k},0)]^*\rangle=0$ since the fluctuations in the concentration and total number density are uncoupled at $t=0$ and that $F_j^{\mathrm{trans}}(k,t=0)=1$. In hydrodynamics ($k\to 0$) the fluctuations in the concentration c and the total number density N are uncoupled for all times t, implying that $F_{cN}(k,t)=0$ for all t. We assume that this decoupling property holds also for the finite k values relevant in this paper. Hence the experimental spectrum $S_{\mathrm{expt}}(k,\omega)$ is the sum of two coherent contributions due to fluctuations in the concentration c and the total number density N and two incoherent contributions due to the rotational and translational motion of single molecules of species $j=1,2$. The k behavior of the total coherent intensity

$$I^{\mathrm{coh}}(k)=[C_c(k)]^2S_{cc}(k)+[C_N(k)]^2S_{NN}(k) \tag{25}$$

to $S_{\mathrm{expt}}(k)$ in Eq. (24) can be estimated easily using the so-called contrast or continuum approximation, discussed in the following subsection.

B. Continuum approximation

In the continuum approximation[10,12], for $I^{\mathrm{coh}}(k)$ the details of the large molecule ($j=1$) are taken into account exactly, but the smaller molecules ($j=2$) are replaced by a continuum background ("medium" or "solvent"). One starts from Eq. (8) for $I^{\mathrm{coh}}(k)=I^{\mathrm{coh}}(k,t=0)$, which is, for $k\neq 0$, equivalently given by

$$I^{\mathrm{coh}}(k)=\frac{1}{Nb^2}\left\langle \left| \int_V d\mathbf{R}\,\rho(\mathbf{R})\exp(i\mathbf{k}\cdot\mathbf{R}) \right|^2 \right\rangle . \tag{26}$$

Here $\rho(\mathbf{R})$ is the scattering length density at $\mathbf{R}$ in the volume V given by

$$\rho(\mathbf{R})=\sum_{j=1,2} f_j^{\mathrm{coh}}(k)\sum_{p=1}^{N_j}\delta(\mathbf{R}-\mathbf{R}_{j,p}) . \tag{27}$$

In the continuum approximation one assumes that $\rho(\mathbf{R})=\rho_m$ is independent of $\mathbf{R}$ when $\mathbf{R}\in V_2$, the volume occupied by the medium. Here ρ_m is the average scattering length density of the medium defined by

$$\rho_m=\frac{1}{V_2}\int_{V_2} d\mathbf{R}\,\rho(\mathbf{R})=n_2 f_2^{\mathrm{coh}}(k) . \tag{28}$$

Then one has in the continuum approximation (CA) for large spherical particles with diameter σ_1

$$I_{\mathrm{CA}}^{\mathrm{coh}}(k)=\frac{x_1}{b^2}[f_1^{\mathrm{coh}}(k)-n_2 v_1 h_1(k) f_2^{\mathrm{coh}}(k)]^2 S_{11}^{\mathrm{CA}}(k) , \tag{29}$$

with $v_l=\pi\sigma_1^3/6$ the volume of a large particle, $h_1(k)$ its normalized form factor

$$h_1(k)\equiv\frac{1}{v_1}\int_{r<\sigma_i/2}d\mathbf{r}\exp(i\mathbf{k}\cdot\mathbf{r})=6j_1(k\sigma_1/2)/(k\sigma_1)\ , \tag{30}$$

where $j_1(x)$ is the spherical Bessel function of order 1, and $S_{11}^{\mathrm{CA}}(k)$ is the partial static structure factor of the large particles in the continuum approximation (i.e., in the absence of the medium particles). Thus $S_{11}^{\mathrm{CA}}(k)$ is equal to the static structure factor of N_1 hard spheres with diameter σ_1 in vacuum in a volume V.

The expressions for $I^{\mathrm{coh}}(k)$ given by Eqs. (25) and (29) are the same if one also uses the continuum approximations $S_{12}^{\mathrm{CA}}(k)$ and $S_{22}^{\mathrm{CA}}(k)$ for the partial structure factors $S_{12}(k)$ and $S_{22}(k)$, which appear in the expressions for $C_c(k)$, $C_N(k)$, $S_{cc}(k)$, and $S_{NN}(k)$. These can be derived from Eq. (14) in a manner completely similar to that described above for $I_{\mathrm{CA}}^{\mathrm{coh}}(k)$, with the result

$$\begin{aligned}S_{12}^{\mathrm{CA}}(k)&=-\left[\frac{x_1}{x_2}\right]^{1/2}n_2v_1h_1(k)S_{11}^{\mathrm{CA}}(k)\ ,\\ S_{22}^{\mathrm{CA}}(k)&=\frac{x_1}{x_2}[n_2v_1h_1(k)]^2S_{11}^{\mathrm{CA}}(k)\ .\end{aligned} \tag{31}$$

Thus we obtain the continuum approximation

$$\begin{aligned}C_c^{\mathrm{CA}}(k)&=\frac{(x_1x_2)^{1/2}}{b}\frac{f_1^{\mathrm{coh}}(k)-n_2v_1h_1(k)f_2^{\mathrm{coh}}(k)}{x_2+x_1n_2v_1h_1(k)}\ ,\\ S_{cc}^{\mathrm{CA}}(k)&=\frac{1}{x_2}[x_2+x_1n_2v_1h_1(k)]^2S_{11}^{\mathrm{CA}}(k)\ ,\\ S_{NN}^{\mathrm{CA}}(k)&=0\ .\end{aligned} \tag{32}$$

Therefore,

$$I_{\mathrm{CA}}^{\mathrm{coh}}(k)=C_c^{\mathrm{CA}}(k)^2S_{cc}^{\mathrm{CA}}(k)\ , \tag{33}$$

which is Eq. (25) in continuum approximation. Note that $S_{NN}^{\mathrm{CA}}(k)=0$ so that the intensity $I_{\mathrm{CA}}^{\mathrm{coh}}(k)$ is completely due to concentration fluctuations.

C. C_{60} in CS_2

Here we apply the general results for $S_{\mathrm{expt}}(k,\omega)$ [cf. Eqs. (4) and (22)] and $S_{\mathrm{expt}}(k)$ [cf. Eq. (24)] to the C_{60}-CS_2 mixtures considered in this paper. First we evaluate the coherent angular averaged molecular form factors $f_j^{\mathrm{coh}}(k)$ of Eq. (10). For a C_{60} molecule ($j=1$) one has

$$f_{C_{60}}^{\mathrm{coh}}(k)=60b_Cj_0(kr_C)\ , \tag{34}$$

with $b_C=6.646$ fm the coherent scattering length of one carbon atom, $r_C=0.354$ nm the nuclear cage radius of C_{60} [13], and $j_0(x)$ the spherical Bessel function of order 0. For a CS_2 molecule ($j=2$) one has the form factor

$$F_{CS_2}^{\mathrm{coh}}(k)=b_C+2b_Sj_0(kr_{CS})\ , \tag{35}$$

with $b_S=2.847$ fm the coherent scattering length of one sulphur atom and $r_{CS}=0.155$ nm the distance between the C and S nuclei in the CS_2 molecule.

Next we consider the rotational form factors $F_j^{\mathrm{rot}}(k,t)$ of Eq. (20). Due to the almost perfect spherical symmetry of a C_{60} molecule, one has for $k<25$ nm^{-1} [14] that

$$F_{C_{60}}^{\mathrm{rot}}(k,t)=0\ . \tag{36}$$

For CS_2 one finds for $t=0$ that

$$F_{CS_2}^{\mathrm{rot}}(k)=2\frac{b_S^2}{b^2}[1+j_0(2kr_{CS})-2j_0^2(kr_{CS})]\ , \tag{37}$$

where $F_{CS_2}^{\mathrm{rot}}(k)$ vanishes proportional to k^4 for $k\to0$. We assume that the ellipsoidal shaped CS_2 molecules cannot rotate easily in the mixture so that we take $F_{CS_2}^{\mathrm{rot}}(k,t)=F_{CS_2}^{\mathrm{rot}}(k)$ for all times t relevant for our experiment. Thus, in fact, we have for the experimentally observed dynamic structure factor

$$\begin{aligned}S_{\mathrm{expt}}(k,\omega)&=[C_c(k)]^2S_{cc}(k,\omega)+[C_N(k)]^2S_{NN}(k,\omega)\\ &\quad+x_{CS_2}F_{CS_2}^{\mathrm{rot}}(k)S_{CS_2}^{\mathrm{trans}}(k,\omega)\ ,\end{aligned} \tag{38}$$

with corresponding intensities

$$\begin{aligned}S_{\mathrm{expt}}(k)&=[C_c(k)]^2S_{cc}(k)+[C_N(k)]^2S_{NN}(k)\\ &\quad+x_{CS_2}F_{CS_2}^{\mathrm{rot}}(k)\ .\end{aligned} \tag{39}$$

Therefore $S_{\mathrm{expt}}(k,\omega)$ can be described as a sum of three Lorentzian lines in ω,

$$\begin{aligned}S_{\mathrm{expt}}(k,\omega)&=I_c(k)\frac{\omega_c(k)/\pi}{\omega_c(k)^2+\omega^2}+I_N(k)\frac{\omega_N(k)/\pi}{\omega_N(k)^2+\omega^2}\\ &\quad+I_{CS_2}(k)\frac{\omega_{CS_2}(k)/\pi}{\omega_{CS_2}(k)^2+\omega^2}\ ,\end{aligned} \tag{40}$$

with intensities $I_c(k)=[C_c(k)]^2S_{cc}(k)$, $I_N(k)=[C_N(k)]^2S_{NN}(k)$, and $I_{CS_2}(k)=x_{CS_2}F_{CS_2}^{\mathrm{rot}}(k)$ and half-widths $\omega_c(k)$, $\omega_N(k)$, and $\omega_{CS_2}(k)$, which are the decay rates of (coherent) concentration fluctuations (c) and total number fluctuations (N) and the (incoherent) density fluctuations of one CS_2 molecule (CS_2).

The partial structure factors $S_{ij}(k)$ $(i,j=1,2)$ that appear in the expressions for $C_c(k)$ and $C_N(k)$ [Eq. (17)], and $S_{cc}(k)$ and $S_{NN}(k)$ are calculated with the Percus-Yevick theory for binary mixtures of hard spheres. We determine the effective hard sphere molecular diameters $\sigma_{C_{60}}=0.91$ nm and $\sigma_{CS_2}=0.42$ nm as before [5]. The relevant number densities $n_{C_{60}}$ and n_{CS_2} and mole fractions are summarized in Table II. The partial structure

TABLE II. Properties of the two C_{60}-CS_2 mixtures.

Property \ C_{60} content	7.9 mg/ml	4.0 mg/ml
$n_{C_{60}}$ (nm^{-3})	6.7×10^{-3}	3.4×10^{-3}
n_{CS_2} (nm^{-3})	10.0	10.0
$x_{C_{60}}$	6.7×10^{-4}	3.4×10^{-4}
b (fm)	7.883	7.828
D_c^E (m^{2}s^{-1})	1.5×10^{-9}	1.5×10^{-9}
$D_{CS_2}^E$ (m^{2}s^{-1})	7×10^{-9}	7×10^{-9}

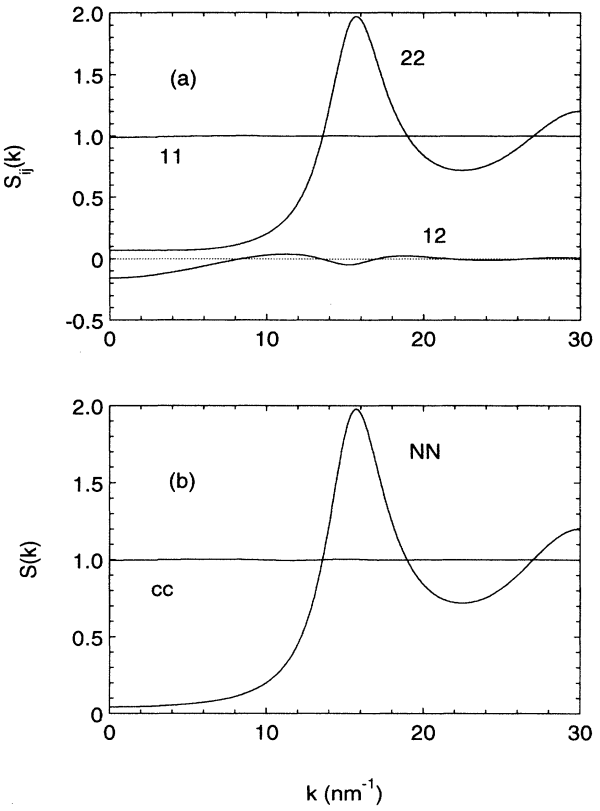

FIG. 6. Static structure factors as functions of k from the Percus-Yevick theory for a hard sphere mixture representing C_{60} in CS_2 at 7.9 mg/ml. (a) $S_{11}(k), S_{22}(k), S_{12}(k)$ [cf. Eq. (14)]; (b) $S_{cc}(k), S_{NN}(k)$. Note that $S_{11}(k) \approx S_{cc}(k) \approx 1$ and $S_{22}(k) \approx S_{NN}(k)$.

factors $S_{ij}(k)$ $(i,j=1,2)$ and $S_{cc}(k)$ and $S_{NN}(k)$ are plotted in Fig. 6 for the mixture with 7.9 mg/ml. Since $x_1 = x_{C_{60}} = 6.7 \times 10^{-4}$ is very small, one sees that $S_{11}(k) = 1 + O(x_2)$ and $S_{cc}(k) = 1 + O(x_1)$ are practically indistinguishable from 1 (cf. Fig. 6). However, deviations of $S_{12}(k)$ from zero are clearly observed since for $x_1 \to 0$, $S_{12}(k)$ is proportional to $x_1^{0.5}$ $(=0.026)$. These significant deviations are enlarged in Fig. 7, where we show the reduced cross correlation function

$$s_{12}(k) \equiv -\left[\frac{x_2}{x_1}\right]^{0.5} S_{12}(k) , \tag{41}$$

which is independent of x_l for small x_1 (including $x_1 = 0$). In Fig. 6, $S_{NN}(k)$ and $S_{22}(k) = S_{NN}(k) + O(x_1)$ [cf. Eq. (13)] are determined almost completely by the CS_2 particles and show the features typical for a dense single-component fluid of particles $(x_1 = 0)$, i.e., a sharp maximum near $k = 2\pi/\sigma_{CS_2} = 15$ nm^{-1}, while $S_{NN}(k) \ll 1$ for $k \ll 2\pi/\sigma_{CS_2}$ due to the low compressibility of a dense fluid. We have shown before that the theoretical $S_{NN}(k)$ given in Fig. 6(b) agrees very well with the experimental $S_{NN}(k)$ obtained from neutron diffraction on pure CS_2 [5]. The intensities $I_c(k)$, $I_N(k)$, and $I_{CS_2}(k)$ are plotted

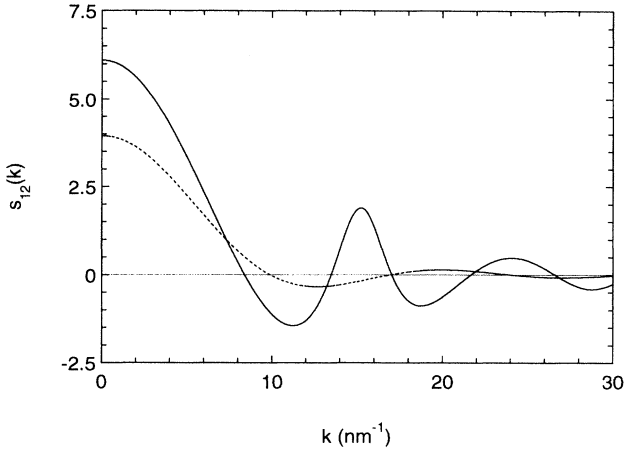

FIG. 7. Reduced hard sphere cross correlation functions $s_{12}(k)$ [cf. Eq. (41)] as functions of k for C_{60} in CS_2 at 7.9 mg/ml. Solid curve, Percus-Yevick theory, dashed curve, continuum approximation [Eq. (31)].

in Fig. 8(a). Using that x_1 is small one finds that

$$\begin{aligned} I_c(k) &= \frac{x_1}{b^2}\{f_1^{\rm coh}(k) - f_2^{\rm coh}(k)[S_{NN}(k) + s_{12}(k)]\}^2 \\ &\quad + O(x_1^2) , \\ I_N(k) &= \frac{1}{b^2} f_2^{\rm coh}(k)^2 S_{NN}(k) + O(x_1) , \\ I_{CS_2}(k) &= F_{CS_2}^{\rm rot}(k) + O(x_1) , \end{aligned} \tag{42}$$

where $s_{12}(k)$ is defined by Eq. (41) and correction terms of higher order in x_1 are irrelevant here. For small k, $f_1^{\rm coh}(k) = 50.6b[1 - (kr_{CS})^2/6 + O(k^4)]$ and $f_2^{\rm coh}(k) = 1.565b[1 - 0.077(kr_{CS})^2 + O(k^4)]$ [cf. Eqs. (34) and (35) and Table II]. Thus, as one observes in Fig. 8, $I_c(k)$ is the dominant contribution to the total intensity for $k \le 5$ nm^{-1}. For $k > 5$ nm^{-1}, $I_N(k)$ starts to dominate due to the decrease of $I_c(k)$ and the increase of $S_{NN}(k)$ (cf. Fig. 6).

The incoherent intensity $I_{CS_2}(k) \sim k^4$ is negligible for small k and contributes significantly to the total intensity only for $k \ge 20$ nm^{-1} (cf. Fig. 8). One also sees in Fig. 8 that the intensity $I_c(k)$ is reasonably well represented by its continuum approximation $I_{CA}^{\rm coh}(k)$ [cf. Eq. (29), with $S_{11}^{CA}(k) = 1$]. The reason is that both are dominated by the same leading contribution $x_1[f_1^{\rm coh}(k)/b]^2$. The significant difference between $I_c(k)$ and $I_{CA}^{\rm coh}(k)$ is due, first, to the fact that for $I_c(k)$, $S_{NN}(k) \neq 0$ (cf. Fig. 6) while $S_{NN}^{CA}(k) = 0$ for $I_{CA}^{\rm coh}(k)$ [cf. Eq. (32)]. Second, $s_{12}(k)$ in Eq. (41) differs from its continuum approximation $s_{12}^{CA}(k)$, given by Eqs. (31) and (41), i.e., $s_{12}^{CA}(k) = n_2 v_1 h_1(k)$. This is shown in Fig. 7 for $s_{12}(k)$, where also $s_{12}^{CA}(k)$ is plotted. One has for small k

$$\begin{aligned} I_c(k) &= I_c(0)[1 - \tfrac{1}{3}(kR_g)^2 + O(k^4)] , \\ I_c^{CA}(k) &= I_c^{CA}(0)[1 - \tfrac{1}{3}(kR_g^{CA})^2 + O(k^4)] , \end{aligned} \tag{43}$$

where R_g is by definition the radius of gyration of the C_{60}

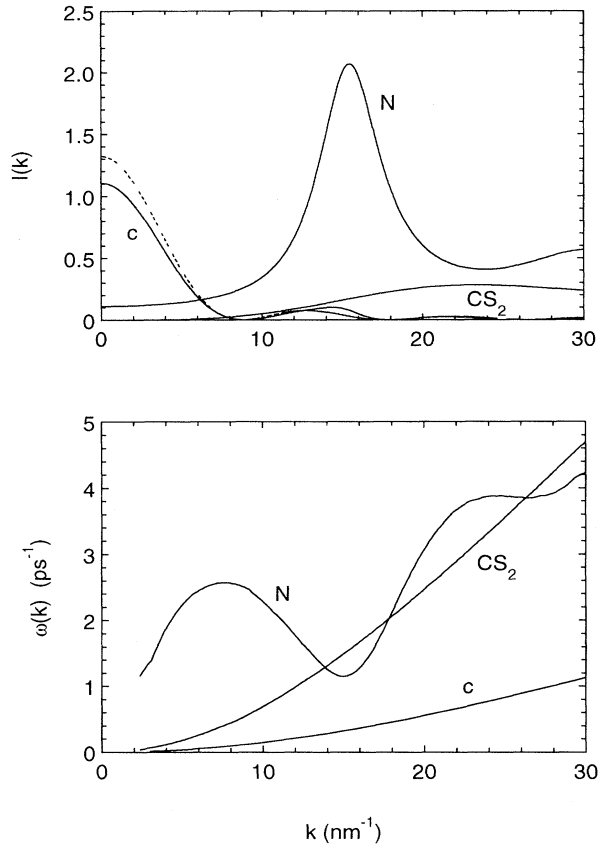

FIG. 8. (a) Neutron intensities $I(k)$ and (b) halfwidths $\omega(k)$ as functions of k for a hard sphere mixture representing C_{60} in CS_2 at 7.9 mg/ml. (a) Solid curves, $I_c(k)$, $I_N(k)$, and $I_{CS_2}(k)$ from Percus-Yevick theory; dashed curve, $I_c(k)$ from the continuum approximation [cf. Eq. (29)]. (b) Solid curves, $\omega_N(k)$, $\omega_{CS_2}(k)$, and $\omega_c(k)$ from the Enskog theory.

molecule [10]. We find $I_c(0)=1.11$ and $I_{CA}^{coh}(0)=1.32$ (cf. Fig. 8), and $R_g=0.994r_C$ and $R_g^{CA}=0.995r_C$, with r_C the nuclear cage radius of C_{60}. It appears therefore that the continuum approximation describes the gyration radius R_g in $I_c(k)$ very accurately (within 1%), but not the initial value $I_c(0)$.

We have calculated the half-widths $\omega_c(k)$,$\omega_N(k)$, and $\omega_{CS_2}(k)$ of Eq. (40) using the revised Enskog theory for binary mixtures of hard spheres [2]. To do so, one needs the partial structure factors $S_{ij}(k)$, which we take from the Percus-Yevick theory. The results are shown in Fig. 8(b). One sees that for all k the decay rates of concentration fluctuations $\omega_c(k)$ are much smaller than those for fluctuations in the total density $\omega_N(k)$. Furthermore, for $k<13$ nm^{-1} the incoherent decay rate $\omega_{CS_2}(k)$ of one CS_2 molecule is smaller than the decay rate of fluctuations in the total density since $\omega_N(k)\approx\omega_{CS_2}(k)/S_{NN}(k)$ [1]. For $k>13$ nm^{-1}, $\omega_N(k)$ and $\omega_{CS_2}(k)$ become of the same order. For $k\leq 13$ nm^{-1} the frequencies $\omega_c(k)$ and $\omega_{CS_2}(k)$ are proportional to k^2 and given by

$$\omega_c(k)=D_c^E k^2,\quad \omega_{CS_2}(k)=D_{CS_2}^E k^2\ , \tag{44}$$

where the Enskog diffusion coefficients D_c^E and $D_{CS_2}^E$ are for $x_1\to 0$ given by

$$D_c^E=\frac{3(k_BT)^{0.5}}{8n_2\sigma_{12}^2 g_{12}(\sigma_{12})(2\pi\mu)^{0.5}}\ ,$$
$$D_{CS_2}^E=\frac{3(k_BT)^{0.5}}{8n_2\sigma_2^2 g_{22}(\sigma_{22})(2\pi m_2)^{0.5}}\ , \tag{45}$$

where the label 1 refers to C_{60} and 2 to CS_2, μ is the reduced mass ($\mu^{-1}=m_1^{-1}+m_2^{-1}$), and $g_{ij}(r)$ are the partial equilibrium pair correlation functions. Using the Percus-Yevick theory for $g_{12}(\sigma_{12})$ and $g_{22}(\sigma_{22})$, we find $D_c^E=1.5\times10^{-9}$ m^2 s^{-1} and $D_{CS_2}^E=7\times10^{-9}$ m^2 s^{-1}. One notes that the translational motion of one CS_2 molecule ($\sim D_{CS_2}^E$) is about five times faster than that of a C_{60} molecule ($\sim D_c^E$).

We have performed similar theoretical calculations for the 4.0-mg/ml mixture with $x_1=x_{C_{60}}=3.4\times10^{-4}$. The results for the intensities $I_N(k)$ and $I_{CS_2}(k)$ and half-widths $\omega_c(k)$, $\omega_N(k)$, and $\omega_{CS_2}(k)$ are practically the same as for the 7.9-mg/ml mixture with $x_1=6.7\times10^{-4}$, since all these quantities are independent of x_1 for $x_1\to0$. The only (trivial) difference is in the intensity $I_c(k)$, since $I_c(k)$ is proportional to x_1.

D. Comparison with experiment

The intensities $I_c(k)$ of the narrow Lorentzian in $S_{expt}(k,\omega)$ [cf. Eq. (3)] obtained experimentally for the 4.0- and 7.9-mg/ml solutions agree well with the $I_c(k)$ calculated from the Percus-Yevick theory, as shown in Fig. 3. For both solutions the corresponding experimental half-widths $\omega_c(k)$ are in reasonable agreement with the $\omega_c(k)$ calculated from the revised Enskog theory, as can be seen in Figs. 4 and 5. Hence we identify the narrow Lorentzian in $S_{expt}(k,\omega)$ of Eq. (3) with the contribution in $S_{expt}(k,\omega)$ of Eq. (40) due to concentration fluctuations (labeled c). Note, however, that there is a significant difference in diffusion coefficients (cf. Fig. 5). In experiment one finds $\omega_c(k)=D_S k^2$ with $D_s=(1.04\pm0.01)\times10^{-9}$ m^2 s^{-1}, while in the Enskog theory $\omega_c(k)=D_c^E k^2$ with $D_c^E=1.5\times10^{-9}$ m^2 s^{-1}.

The intensity $I_N(k)$ of the broad Lorentzian in $S_{expt}(k,\omega)$ [cf. Eq. (3)] obtained experimentally for the 7.9-mg/ml solution is in agreement with the theoretical $I_N(k)$ calculated for the total number fluctuations, as shown in Fig. 3(a). In particular, the strong increase of the experimental $I_N(k)$ for $k>10$ nm^{-1} is well described by $I_N(k)$ from theory. We remark that the theoretical $I_N(k)$ [cf. Eq. (42)] is determined only by $f_{CS_2}^{coh}(k)$, which is known exactly, and by $S_{NN}(k)$, which agrees by itself with experimental results of pure CS_2. Furthermore, the incoherent intensity $I_{CS_2}(k)$ is much smaller than $I_N(k)$ [cf. Fig. 8(a)] and shows a very different k behavior compared to $I_N(k)$. Therefore we are sure that the broad

Lorentzian in $S_{\text{expt}}(k,\omega)$ is due to total number fluctuations in the mixture and not to incoherent density fluctuations of single CS_2 molecules.

The experimental half-widths $\omega_N(k)$ (cf. Fig. 4) appear to be much smaller than the Enskog results for $\omega_N(k)$ [cf. Fig. 8(b)]. In fact, the experimental $\omega_N(k)$ behave more like the theoretical half-widths $\omega_{CS_2}(k)$ of incoherent CS_2 fluctuations, as shown in Fig. 4. This suggests that for the CS_2 solvent $\omega_N(k)\approx\omega_{CS_2}(k)$ not only for $k>13$ nm^{-1}, but also for $k<12$ nm^{-1}. The reason for this is unclear at present.

IV. DISCUSSION

The experimental dynamic structure factor $S_{\text{expt}}(k,\omega)$ obtained from neutron scattering for $1\le k\le 15$ nm^{-1} for dilute suspensions of C_{60} molecules in a dense CS_2 liquid consists of one narrow Lorentzian in ω with intensity $I_c(k)$ and half-width $\omega_c(k)$ due to concentration fluctuations (c) and a broad Lorentzian with area $I_N(k)$ and half-width $\omega_N(k)$, due to fluctuations in the total number density N [cf. Eq. (3) and Figs. 3–5]. The incoherent scattering due to the CS_2 molecules proportional to $I_{CS_2}(k)$ in Eq. (40) for $S_{\text{expt}}(k,\omega)$ is too weak to be detected in this k region. We first discuss the results for the intensities $I_c(k)$ and $I_N(k)$. We find that the k behavior of $I_c(k)$ and $I_N(k)$ can be understood very well on the basis of the Percus-Yevick theory for the partial structure factors $S_{ij}(k)$ of binary mixtures of hard spheres of species $j=1,2$, which have neutron form factors $f_1^{\text{coh}}(k)$ and $f_2^{\text{coh}}(k)$ as the actual C_{60} and CS_2 molecules, respectively [cf. Fig. 3(a)]. Like one usually does in small-angle neutron scattering (SANS), we also present our data for $I_c(k)$ in a "Guinier plot" [15] (cf. Fig. 9), i.e., we show $\ln(I(k))$ as a function of k^2, for which one has $\ln(I(k))=\ln(I(0))-(kR_g)^2/3+O(k^4)$ at small k [cf. Eq. (43)]. One observes in Fig. 9 that $\ln(I(k))$ is linear in k^2 up to about $k^2=30$ nm^{-2}. In the inset of Fig. 9 we show a best linear fit in this k^2 region leading to $R_g=0.35\pm0.02$ nm, in perfect agreement with the nuclear cage radius $r_c=0.355$ nm of C_{60} reported in the literature [13]. We remark that $R_g=r_C$ within 1%, also in the continuum approximation, as discussed in Sec. III C. Recently, Affholter *et al.* [16] studied by SANS the static structure of dilute suspensions of C_{60} in liquid CS_2 at room temperature and concentrations of 7.75 and 5.45 mg/ml, which are comparable to ours. They report Guinier plots for $\ln(I_c(k))$ and $k^2\le 10$ nm^{-2} and derive from the slope a radius $R_g=0.382$ nm. Using their data for $\ln(I_c(k))$ versus k^2 in the linear k^2 region, we find that the uncertainty in R_g is at least 10%. Therefore Affholter's result for R_g (0.382 ± 0.04 nm) is consistent with the value found here (0.35 ± 0.02 nm).

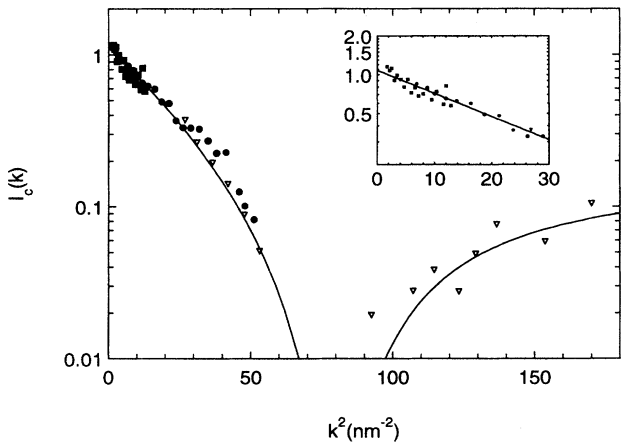

FIG. 9. Neutron intensity $I_c(k)$ as a function of k^2 for C_{60} in CS_2 at 7.9 mg/ml. Experiment, MC002 (■), MC004 (●), and PG002 (▽); Percus-Yevick theory, solid line. $\ln[I(k)]$ is linear in k^2 up to $k^2=30$ nm^{-2} (inset).

Second, we discuss the results for the half-widths $\omega_c(k)$ of the narrow Lorentzian in $S_{\text{expt}}(k,\omega)$. We find that $\omega_c(k)$ is quadratic in k, $\omega_c(k)=D_S k^2$, with a diffusion coefficient $D_S=(1.04\pm0.01)\times10^{-9}$ $\text{m}^2\,\text{s}^{-1}$, significantly smaller than the Stokes-Einstein value $D_{\text{SE}}=1.3\times10^{-9}$ $\text{m}^2\,\text{s}^{-1}$ [Eq. (1)] and the Enskog value $D_c^E=1.5\times10^{-9}$ $\text{m}^2\,\text{s}^{-1}$. It appears therefore that for C_{60} molecules in CS_2 both descriptions have some relevance but are not very accurate.

To investigate whether such differences are systematic we consider the diffusion coefficients D_S of C_{60} molecules in toluene, benzene, and carbon tetrachloride obtained recently by Castillo, Garza, and Ramos from the Taylor dispersion technique [17]. In Table III we compare D_S with the Stokes-Einstein values D_{SE} [Eq. (1) with η from Table III] and the Enskog values D_c^E [Eq. (45)] using $\sigma_{C_{60}}=0.91$ nm, $\sigma_{CS_2}=0.42$ nm, $\sigma_{\text{toluene}}=0.54$ nm, $\sigma_{\text{benzene}}=0.51$ nm, and $\sigma_{CCl_4}=0.53$ nm. Here the effective hard sphere diameters of toluene, benzene, and CCl_4 are rough estimates using that for typical liquids the reduced density $n\sigma^3=0.9$. One observes in Table III that D_S of benzene is exceptionally large. The reason for this is unclear. The theoretical Enskog values D_c^E of toluene, CCl_4, and CS_2 are systematically larger than the experimental values D_S. For toluene and CCl_4, Stokes-Einstein D_{SE} is somewhat smaller than D_S while for Cs_2, D_{SE} is larger than D_S. It appears systematically that Stokes-Einstein agrees better with experiment than Enskog but both descriptions are insufficient. It would clearly be of interest to consider the continuous interactions of the C_{60} molecules with the solvent particles to possibly understand the differences. For C_{60} in CS_2 we expect attractive interactions of C_{60} with CS_2 that make the diffusion coefficient D_S smaller than Stokes-Einstein D_{SE} due to a larger drag of the C_{60} molecules. Attractive interactions between C_{60} and CS_2 are indicated by very recent intermediate angle neutron diffraction experiments on C_{60}-CS_2 systems [18] and are consistent with the anomalous large solubility of C_{60} in CS_2 [6]. For C_{60} in toluene the interactions are negligible while for C_{60} in CCl_4 they are possibly repulsive. We remark that interactions between two C_{60} molecules in the CS_2 solvent are irrelevant. This follows from the fact that $\omega_c(k)=D_S k^2$ is perfectly quadratic in k and D_S is independent of the C_{60} concentration

TABLE III. Stokes-Einstein D_{SE} and Enskog D_c^E and experimental diffusion coefficients D_S for C_{60} in various solvents.

Solvent	T (K)	η (10^{-3} kg m^{-1} s^{-1})	D_{SE} (10^{-9} m^2 s^{-1})	D_c^E (10^{-9} m^2 s^{-1})	D_S (10^{-9} m^2 s^{-1})
toluene	303	0.526	0.93	1.5	0.97±0.04[a]
benzene	303	0.564	0.86	1.4	2.38±0.03[a]
CCl_4	303	0.843	0.57	1.1	0.80±0.12[a]
CS_2	293	0.363	1.30	1.5	1.04±0.01

[a]Reference [17].

(cf. Fig. 5).

Finally, we note that the half-width $\omega_N(k)$ of the broad Lorentzian in $S_{expt}(k,\omega)$ is much smaller than that calculated from the Enskog theory [cf. Figs. 4 and 8(b)]. It is clearly important to test the validity of the Enskog theory for $\omega_N(k)$ for one-component molecular fluids, which have not been done so far.

A brief report of a part of the present experiment has been given before [5]. There we use the (at that time) standard ISIS tables for the detector angles ϕ of the IRIS spectrometer to convert the spectra from constant ϕ to constant wave number k. In the present paper we use the detector angles ϕ as found in a new calibration experiment, which are slightly different. This is the source of small but systematic differences for the half-widths $\omega_c(k)$ presented before [5] and shown here as part of the results.

ACKNOWLEDGMENTS

We acknowledge financial support from the Netherlands Organisation for Scientific Research (NWO) and the useful discussions with M. A. Adams, W. S. Howells, and D. S. Sivia.

[1] P. N. Pusey, in *Liquids, Freezing and Glass Transition,* 1989 Les Houches Lectures, Session LI, edited by J. P. Hansen, D. Levesque, and J. Zinn-Justin (North-Holland, Amsterdam, 1991).

[2] H. van Beijeren and M. H. Ernst, Physica **68**, 437 (1973); **70**, 225 (1973); J. Stat. Phys. **21**, 125 (1979).

[3] P. Westerhuijs, L.A. de Graaf, and I. M. de Schepper, Phys. Rev. E **48**, 1948 (1993); H. E. Smorenburg, L. A. de Graaf, and I. M. de Schepper, Phys. Lett. A **181**, 321 (1993).

[4] J. R. Dorfman and H. van Beijeren, in *Statistical Mechanics B,* edited by B. J. Berne (Plenum, New York, 1977).

[5] H. E. Smorenburg, I. M. de Schepper, and L. A. de Graaf, Phys. Lett. A **187**, 204 (1994).

[6] N. Sivaraman, R. Dhamodaran, I. Kaliappan, T. G. Srinivasan, P. R. Vasudeva Rao, and C.K. Mathews, J. Org. Chem. **57**, 6077 (1992); R. S. Ruoff, D. S. Tse, R. Malhotra, and D. C. Lorents, J. Phys. Chem. **97**, 3379 (1993); R. S. Ruoff, R. Malhotra, D. L. Huestis, D. S. Tse, and D. C. Lorents, Nature **362**, 140 (1993).

[7] *CRC Handbook of Chemistry and Physics,* edited by R. C. Weast, 62nd ed. (CRC, Boca Raton, FL, 1982).

[8] C. J. Carlile and M. A. Adams, Physica B **182**, 431 (1992).

[9] H. Fredrikze, Ph.D. thesis, Delft University of Technology, 1985 (unpublished).

[10] S. W. Lovesey, *Theory of Neutron Scattering from Condensed Matter* (Clarendon, Oxford, 1984), Vol. 1.

[11] A. B. Bathia and D. E. Thornton, Phys. Rev. B **2**, 3004 (1970).

[12] D. L. Price and K. Sköld, in *Methods of Experimental Physics, Neutron Scattering,* edited by K. Sköld and D. L. Price (Academic, New York, 1986), Vol. 23A.

[13] K. Prassides and H. Kroto, Phys. World April, 44 (1992).

[14] D. A. Neumann, J. R. D. Copley, R. L. Cappeletti, W. A. Kamitakahara, R. M. Lindstrom, K. M. Creegan, D. M. Cox, W. J. Romanow, N. Coustel, J. P. McCauley, Jr., N. C. Maliszewskyj, J. E. Fischer, and A. B. Smith, Phys. Rev. Lett. **67**, 3808 (1991).

[15] A. Guinier and G. Fournet, *Small Angle Scattering of X-Rays* (Wiley Interscience, New York, 1955).

[16] K. A. Affholter, S. J. Henderson, G. D. Wignall, G. J. Bunick, R. E. Haufler, and R. N. Compton, J. Chem. Phys. **99**, 9224 (1993).

[17] R. Castillo, C. Garza, and S. Ramos, J. Phys. Chem. **98**, 4188 (1994).

[18] S. Spooner, J. L. Zarestky, and K. A. Affholter (unpublished).